Self-organized nanocolumnar structure in superhard TiB_2 thin films

P. H. Mayrhofer[a] and C. Mitterer
Department of Physical Metallurgy and Materials Testing, University of Leoben, A-8700 Leoben, Austria

J. G. Wen, J. E. Greene, and I. Petrov
Frederick Seitz Materials Research Laboratory and Department of Materials Science, University of Illinois, Urbana, Illinois 61801

(Received 13 October 2004; accepted 16 February 2005; published online 21 March 2005)

TiB_2 thin films are well known for their high hardness which makes them useful for wear-resistant applications. Overstoichiometric TiB_2 deposited at 300 °C by nonreactive sputtering has been shown to exhibit superhardness ($H \geqslant 40$ GPa), while the hardness of their bulk stoichiometric counterparts is ~25 GPa. We show, using high-resolution transmission electron microscopy, that overstoichiometric $TiB_{2.4}$ layers have a complex self-organized columnar nanostructure. The ~20 nm wide columns, encapsulated in excess B and oriented along 0001, consist of a bundle of ~5 nm diameter TiB_2 subcolumns separated by an ultrathin B-rich tissue phase. The nanocolumnar structure, which is thermally stable to postannealing temperatures up to 700 °C, inhibits nucleation and glide of dislocations during hardness indentation measurements, while the high cohesive strength of the B-rich tissue phase prevents grain-boundary sliding. The combination of these effects results in the observed superhardness of ~60 GPa. © *2005 American Institute of Physics*. [DOI: 10.1063/1.1887824]

TiB_2 thin films, and transition-metal nitrides and carbides containing TiB_2, have been studied extensively due to their high hardness and thermochemical stability.[1–6] Their properties are highly attractive for a wide range of applications in erosive, abrasive, corrosive, and/or high-temperature environments.[3] TiB_2 crystallizes in the hexagonal C32 structure in which B is located in the interstices between (0001) close-packed Ti planes.[1,7] Thus, B and Ti planes alternate along the c axis.[1,7] Reported lattice parameters are $a = 0.3038$ nm and $c = 0.3220$ nm.[8–10] Due primarily to the strong covalent bonding in the B network, TiB_2 has a relatively narrow single-phase field with a composition ranging from 65.6 to 66.7 at. % B, a high melting point (3225 °C), and a high hardness ($H = 25$ GPa).[7,10]

Recently, TiB_2 thin films deposited by *nonreactive* dc sputtering from compound targets have been shown to have much higher hardnesses, 48 to 77 GPa, which are not simply due to correspondingly high residual stresses.[1,4] However, the mechanism giving rise to this superhardness effect (defined in Ref. 11 as $H \geqslant 40$ GPa) is not understood. While it has been speculated that the nanostructure and grain boundaries of the film may play an important role,[1,4] these features have not been investigated in detail. A review of the literature reveals that superhard TiB_2 is only obtained in overstoichiometric layers with a pronounced 0001 texture.[1–4,6]

Here, we use high-resolution transmission electron microscopy (HRTEM) to show that superhard overstoichiometric TiB_2 films have a columnar structure, with an average feature size of ~20 nm, and 0001 preferred orientation. The columns are encapsulated in excess B and are themselves composed of smaller stoichiometric TiB_2 subcolumns with an average diameter of ~5 nm, separated by a thin B-rich tissue phase of thickness 1–2 monolayers (ML). Due to the small dimension across the TiB_2 nanocolumns, nucleation and glide of dislocations is inhibited during hardness indentation measurements, while the high cohesive strength of the thin B-rich tissue phase prevents grain-boundary sliding. Together, these two effects explain the observed superhardness of overstoichiometric TiB_2 layers.

TiB_2 films, 3 μm thick, are grown on austenitic stainless steel and Si(001) substrates at 300 °C by magnetically unbalanced magnetron sputter deposition from a stoichiometric TiB_2 target (150 mm in diameter) in Ar (99.999% purity) discharges. The Ar pressure and power density are 0.4 Pa (3×10^{-3} Torr) and 3.5 W cm^{-2}, respectively, yielding a deposition rate R of 0.56 nm s^{-1}. The deposition system and growth conditions are described in more detail in Ref. 2. The incident metal flux J_{Ti} is estimated based upon measurements of the deposition rate, film composition (see next paragraph), and film thickness and assuming bulk density. The ion flux J_{Ar^+} and the ion energy E_{Ar^+} bombarding the growing film are determined using Langmuir-probe measurements following the procedures described in Ref. 12. E_{Ar^+} is maintained constant at 30 eV in these experiments. As-deposited films are annealed in a vacuum at temperatures T_a of 500, 600, and 700 °C at pressures $\leqslant 10^{-3}$ Pa(7.5×10^{-6} Torr) for 1 h.

Film compositions are measured by wavelength dispersive electron probe microanalyses calibrated using a stoichiometric TiB_2 standard whose composition was determined by nuclear reaction analyses. B/Ti ratios x in as-deposited films were found to depend strongly on the incident ion/metal flux ratio (J_{Ar^+}/J_{Ti}) during growth with $x = 2.4$, 3.0, and 3.2 for $J_{Ar^+}/J_{Ti} = 0.4$, 6, and 12, respectively. The films exhibit no detectable impurities within the detection limit of approximately 0.1 at. %.

The biaxial compressive stress σ, measured using the cantilever beam method,[5] in films grown on Si(001) ranges from −0.03 GPa with $x = 2.4$ to −1.82 GPa with $x = 3.0$ to −2.40 GPa with $x = 3.2$. The thermal expansion coefficient of overstoichiometric TiB_x films is $\sim 6.5 \times 10^{-6}$ K^{-1},[5] giving rise to differential thermal contraction stresses, upon cooling from the growth temperature, of +0.90 GPa on Si(001) and

[a]Electronic mail: paul.mayrhofer@unileoben.ac.at

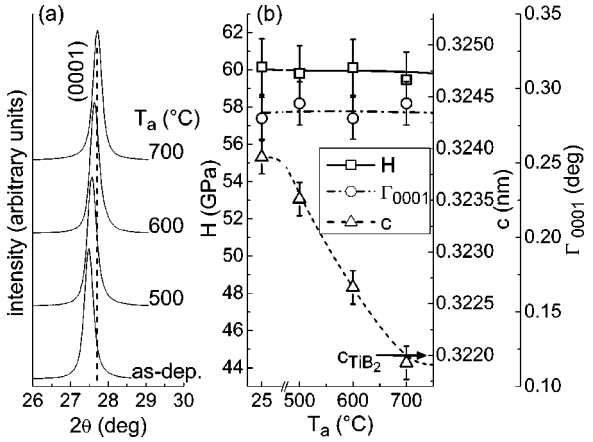

FIG. 1. (a) XRD patterns from an as-deposited $TiB_{2.4}$ film and samples which have been annealed for 1 h at temperatures T_a. (b) Hardness H, lattice constant c, and full width at half maximum Γ of the (0001) XRD reflection as a function of T_a. For comparison, the lattice constant c of TiB_2 is indicated by an arrow.

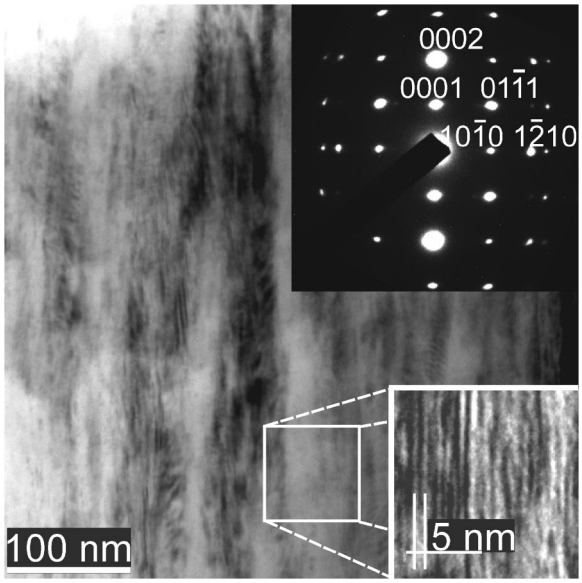

FIG. 2. Bright-field XTEM image, with a corresponding SAED pattern obtained near the upper portion, of a $TiB_{2.4}$ layer after annealing at 700 °C. The inset is a higher-resolution image showing the 0001-oriented ~5 nm wide subcolumnar nanostructure.

−3.10 GPa on the steel substrates. Combining the results of the cantilever measurements with the thermal contraction stresses, the intrinsic stresses during growth are estimated to be −0.93 GPa with $x=2.4$, −2.72 GPa with $x=3.0$, and −3.30 GPa with $x=3.2$. Hardnesses H of the films on steel substrates are obtained by computer-controlled measurements using a Fischerscope H100C with a 50 mN load for which the Vickers indentation depth is ⩽10% of the film thickness. H values for all of our overstoichiometric TiB_x films, irrespective of x or σ, remain constant at 60±3 GPa.

Here, we focus on films with $x=2.4$ which have low macrostress as deposited. The nanostructures of these layers in both the as-deposited and annealed states are determined using Bragg–Brentano x-ray diffraction (XRD) with Cu $K\alpha$ radiation, transmission electron microscopy (TEM), and electron energy-loss spectroscopy (EELS). There are no detectable differences in nanostructure and texture between the $TiB_{2.4}$ films grown on steel and Si(001).

The only XRD peaks obtained from as-deposited and annealed $TiB_{2.4}$ layers grown on steel substrates over the 2θ range 20°–90° are the 0001 at 27.54° [see Fig. 1(a)] and the 0002 at 56.94°. The 0001 peak position continuously shifts from 27.54° (lattice constant $c=0.3239$ nm) in the as-deposited state to 27.71° ($c=0.3219$ nm) after annealing at 700 °C as indicated in Figs. 1(a) and 1(b). The lattice constant in the [0001] direction for bulk TiB_2 is $c_0=0.3220$ nm.[9,10] Thus, the $TiB_{2.4}$ films exhibit compressive macrostrain in the as-deposited state ($c>c_0$), changing to an essentially unstrained condition after annealing at 700 °C [see Fig. 1(b)]. The full width at half maximum intensity Γ_{0001} of the 0001 reflection remains constant at 0.28°±0.01° as a function of annealing temperature for $T_a \leqslant 700$ °C [Fig. 1(b)] suggesting that there are no significant changes in either the nanostructure or local lattice microstrain[13] as a function of annealing.

Increased diffusivities during film annealing commonly lead to defect annihilation and atomic rearrangement resulting in lower stresses.[14,15] Since structural defects act as obstacles for dislocation motion, a direct relationship between defect density and hardness is expected.[15] Thus, both diffraction peak widths Γ and the hardness of stoichiometric binary nitride and carbide layers typically decrease during annealing.[16,17] However, in the present experiments carried out on overstoichiometric $TiB_{2.4}$, we observe that while the film lattice constant (and hence macrostress) decreases with annealing temperature $T_a \leqslant 700$ °C, Γ and H remain constant [see Fig. 1(b)].

TEM investigations reveal no observable differences in the nanostructure of as-deposited $TiB_{2.4}$ layers and samples which were annealed at 700 °C. This is consistent with the XRD results showing that Γ_{0001} remains constant with T_a. Figure 2 is a bright-field cross-sectional TEM (XTEM) image with a corresponding selected area electron diffraction (SAED) pattern from a $TiB_{2.4}$ layer annealed at 700 °C. The film has a dense columnar structure with an average column diameter of ~20 nm and a smooth surface with an average root-mean-square roughness essentially equal to that of the polished substrate surface, ~15 nm. SAED patterns obtained as a function of film thickness show an 0001 texture near the film/substrate interface with increased preferred orientation near the film surface. The 20 nm diameter columns are composed of bundles of subcolumns, with an average coherence length of ~5 nm, which extend along the film growth direction (see inset in Fig. 2) throughout the entire coating thickness. The feature spacing does not change with imaging diffraction vector showing that the contrast is not due to Moiré interference fringes. Rather, the modulation results from atomic number and/or strain contrast caused by a lateral compositional variation during film growth, similar to the surface-initiated spinodal decomposition observed in $Ti_{0.5}Al_{0.5}N$.[18] This is verified by high-resolution (HR) XTEM, plan-view TEM, and scanning TEM investigations.

Figure 3 is a HR-XTEM image of a $TiB_{2.4}$ sample after annealing at $T_a=700$ °C. TiB_2 0001 lattice fringes are visible within ~5 nm wide nanocolumns separated by ~0.5 nm thick (1–2 ML) disordered regions, which we refer to as a tissue phase (indicated by the white dashed lines in Fig. 3). The lattice fringe spacing c is consistent with stoichiometric TiB_2. The inset in Fig. 3 is a high-angle annular dark-field (Z-contrast) cross-sectional image with alternating dark and

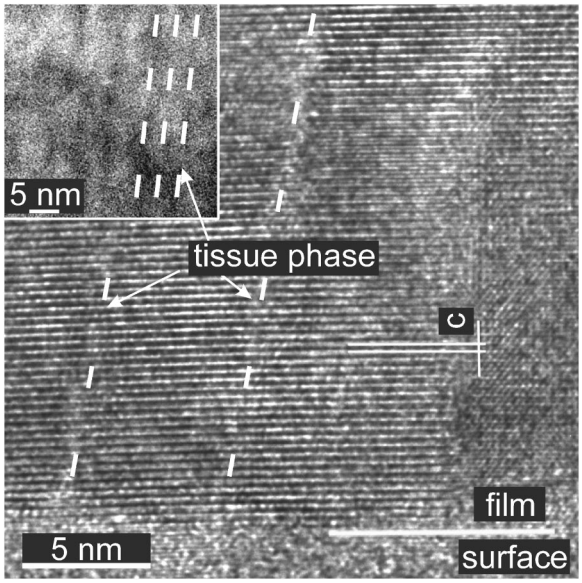

FIG. 3. Bright-field cross-sectional HRTEM image of a $TiB_{2.4}$ layer after annealing at 700 °C. The inset is a lower resolution *Z*-contrast image.

bright stripes. Regions with a lower average atomic number *Z* appear darker and are, therefore, B-rich compared to the brighter TiB_2 regions. As confirmed by plan-view HRTEM investigations (see Fig. 4), the nanostructure is composed of bundles of ~5 nm diameter coherent subcolumns, separated by a thin (~0.5 nm, 1–2 ML) disordered B-rich tissue phase, within ~20 nm wide 0001-oriented columns. Quantitative analyses of EELS measurements obtained from plan-view samples using a 1 nm spot size reveal that the subcolumns are stoichiometric TiB_2 in agreement with the fringe spacing, whereas the disordered regions are highly B rich.

From the above results, we conclude that overstoichiometric $TiB_{2.4}$ layers with excess B exhibit a complex self-organized nanostructure. Columns with 0001 preferred orientation and diameters of ~20 nm are encapsulated in excess B. The columns themselves are composed of bundles of coherent ~5 nm diameter TiB_2 subcolumns that are separated by a disordered 1–2 ML thin B-rich tissue phase. TEM and XRD investigations show that this nanostructure is thermally stable to annealing temperatures up to at least 700 °C, while indentation results show that the film hardness is also unaffected by annealing.

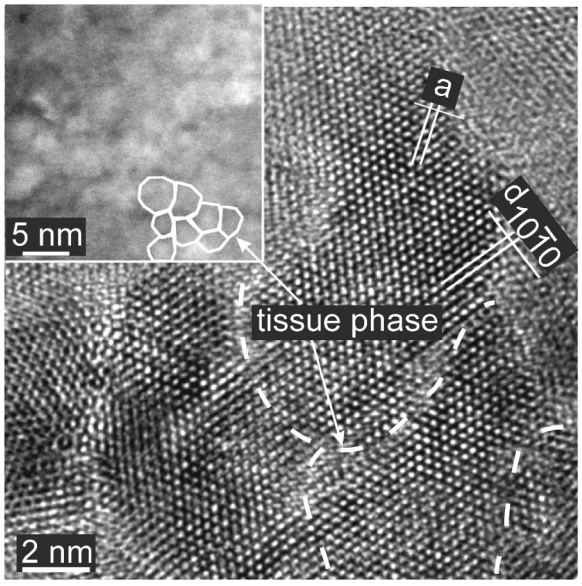

FIG. 4. Bright-field plan-view 0001 HRTEM image of an as-deposited $TiB_{2.4}$ layer. The inset is a lower resolution *Z*-contrast image.

The hardness of a material is determined by resistance to bond distortion and dislocation formation and motion during indentation. The primary dislocation glide planes in our $TiB_{2.4}$ layers are {0001}. However, due to the self-organized nanocolumnar structure, these planes have an average length of only 5 nm. Thus, dislocation formation is unlikely[19] and even if dislocations did nucleate during indentation, the ultrathin (1–2 ML) B-rich tissue phase would act to impede their motion. Furthermore, the cohesive strength of boundary regions, which usually have the lowest resistance to distortion during indentation,[20] is enhanced by the presence of the excess B. Together, these two effects explain the observed superhardness of overstoichiometric $TiB_{2.4}$ layers. Our results are similar to the superhardness achieved with Ti–Si–N nanocomposites[21,22] in which small equiaxed (~5 nm in diameter) TiN clusters are separated by a thin (1–2 ML) amorphous Si_3N_4 boundary layer. A major difference, however, is the anisotropy of our $TiB_{2.4}$ layers which are superhard along the growth direction.

The authors acknowledge the use of the Center for Microanalysis of Materials, University of Illinois, which is partially supported by the U.S. Department of Energy. They are also very grateful to Dr. P. O. Å. Persson for assistance with the TEM investigations and valuable discussions. Three of the authors (J. G. W, I. P, and J. E. G.) are supported by the U.S. Department of Energy, Division of Materials Sciences, under Award No. DEFG02-91ER45439.

[1] M. Berger, L. Karlsson, M. Larsson, and S. Hogmark, Thin Solid Films **401**, 179 (2001).
[2] P. Losbichler and C. Mitterer, Surf. Coat. Technol. **97**, 567 (1997).
[3] C. Mitterer, J. Solid State Chem. **133**, 279 (1997).
[4] F. Kunc, J. Musil, P. H. Mayrhofer, and C. Mitterer, Surf. Coat. Technol. **174**, 744 (2003).
[5] P. H. Mayrhofer and C. Mitterer, Surf. Coat. Technol. **133**, 131 (2000).
[6] R. Wiedemann and H. Oettel, Surf. Eng. **14**, 299 (1998).
[7] *Binary Alloy Phase Diagrams*, edited by T. B. Massalsky (American Society for Metals, Metals Park, Ohio, 1986).
[8] V. Ferrando, D. Marre, P. Manfrinetti, I. Pallecchi, C. Tarantini, and C. Ferdeghini, Thin Solid Films **444**, 91 (2003).
[9] P. Vajeeston, P. Ravindran, C. Ravi, and R. Asokamani, Phys. Rev. B **63**, 045115 (2001).
[10] R. G. Munro, J. Res. Natl. Inst. Stand. Technol. **105**, 709 (2000).
[11] S. Veprek, J. Vac. Sci. Technol. A **17**, 2401 (1999).
[12] I. Petrov, V. Orlinov, I. Ivanov, and J. Kourtev, Contrib. Plasma Phys. **28**, 157 (1988).
[13] *Diffraction Analysis of the Microstructure of Materials*, edited by E. J. Mittemeijer and P. Scardi (Springer, Berlin, 2004).
[14] H. Oettel and R. Wiedemann, Surf. Coat. Technol. **76**, 265 (1995).
[15] *Recrystallization and Related Annealing Phenomena*, edited by F. J. Humphreys and M. Hatherly (Elsevier, Oxford, 1995).
[16] P. H. Mayrhofer, H. Clemens, and C. Mitterer, Z. Metallkd. (2005) in press.
[17] L. Hultman, Vacuum **57**, 1 (2000).
[18] F. Adibi, I. Petrov, L. Hultman, U. Wahlström, T. Shimizu, D. McIntyre, J. E. Greene, and J.-E. Sundgren, J. Appl. Phys. **69**, 6437 (1991).
[19] A. E. Romanov, Nanostruct. Mater. **6**, 125 (1995).
[20] J. Schiøtz, F. D. Di Tolla, and K. W. Jacobsen, Nature (London) **391**, 561 (1998).
[21] S. Vepřek, P. Nesladek, A. Niederhofer, and F. Glatz, Nanostruct. Mater. **10**, 679 (1998).
[22] J. Patscheider, T. Zehnder, and M. Diserens, Surf. Coat. Technol. **146**, 201 (2001).